*Uluslararası İleri Doğa Bilimleri ve Mühendislik Araştırmaları Dergisi*
*Sayı 8, S. 10-25, 4, 2024*

***Araştırma Makalesi***

*International Journal of Advanced Natural Sciences and Engineering Researches*
*Volume 8, pp. 10-25, 4, 2024*

***Research Article***

https://as-proceeding.com/index.php/ijanser
ISSN: 2980-0811

# Enhancing sensitivity of dye-sensitized photovoltaics across low illumination conditions through $TiCl_4$ treatment

Mücella ÖZBAY KARAKUŞ*

[1] *Yozgat Bozok University, Engineering and Architecture Faculty, Yozgat 66100, Türkiye*

*(*mucella.karakus@yobu.edu.tr)*

*(Received:09 April 2024, Accepted: 1 May 2024)*

(2nd International Conference on Scientific and Innovative Studies ICSIS 2024, April 18-19, 2024)

**ATIF/REFERENCE:** Karakuş, M. Ö. (2024). Enhancing sensitivity of dye-sensitized photovoltaics across low illumination conditions through $TiCl_4$ treatment. *International Journal of Advanced Natural Sciences and Engineering Researches*, 8(4), 10-25.

***Abstract*** **–** This study investigates the effect of TiCl4 treatment on the fabrication of Dye-Sensitized Photovoltaics (DSPs) structures using Ruthenizer 535-4TBA (N-712) dye. DSPs are known for their sensitivity to low light levels, making them suitable for sensor applications in environments with reduced illumination. The research compares DSP structures treated with TiCl4 during fabrication to those that did not undergo this treatment. The study aims to analyze the impact of these fabrication methods on energy conversion efficiency and sensor performance.

Electrical measurements were conducted under both standard illumination conditions and gradually reduced low-light conditions across 13 steps as 1000, 500, 250, 100, 50, 25, 10, 5, 2, 1, 0,5, 0,3 and 0,1 W/m2. Results show that DSP efficiency significantly increases under low-light conditions, with the TiCl4-treated sample exhibiting an efficiency of 9.33% under 1000 W/m2 illumination, which rises to 27.5% under 0.1 W/m2. Additionally, electrochemical properties were analyzed using Electrochemical Impedance Spectroscopy (EIS). Parameters such as electron lifetime, rise time, and fall time were determined to characterize the sensors. Response times of approximately 4.1 nanoseconds for T-N712 and 5.3 nanoseconds for N712 were recorded.

In summary, the study demonstrates the potential of TiCl4 treatment in enhancing the sensitivity and performance of DSPs, particularly under low-light conditions. The research provides valuable insights into optimizing DSP fabrication processes for improved energy conversion efficiency and sensor capabilities. These findings contribute to the ongoing development of DSPs for various applications, including sensing in environments with limited illumination.

*Keywords – Low Illumination, Photovoltaics, Dye-Sensitized*

## I. INTRODUCTION

As science and technology continue to advance at an unprecedented pace, the global demand for energy escalates year by year, paralleled by a concerning increase in carbon emissions [1]. This surge in energy needs poses a significant challenge to environmental sustainability, necessitating urgent measures to mitigate its impact. While the onset of the COVID-19 pandemic in 2019 led to a marginal downturn in energy consumption and a notable shift in energy demand from commercial to residential spaces due to

remote work arrangements, the persistent energy consumption of idle spaces during the pandemic remains a pressing issue [1]. Despite these challenges, heightened environmental awareness has prompted a renewed focus on reducing carbon emissions and finding sustainable solutions to meet the escalating energy demand. In this context, the application of solar photovoltaics emerges as a promising avenue for addressing these challenges, offering a clean and renewable energy source with the potential to significantly reduce carbon emissions.

The increasing deployment of solar technology across the globe underscores the growing recognition of solar energy's potential as a key player in the transition to sustainable energy systems [2]. This trend reflects the concerted efforts of governments and industries to embrace renewable energy solutions and reduce reliance on fossil fuels. Moreover, the emergence of novel solar-based power generation systems signifies a paradigm shift towards more efficient and versatile energy technologies [3]. These advancements not only enhance energy production but also contribute to the overall resilience and stability of energy systems, particularly in the face of evolving climate-related challenges.

By systematically analyzing the performance and degradation mechanisms of photovoltaic components, researchers can develop targeted strategies to optimize their longevity and effectiveness. Furthermore, advancements in materials science and engineering enable the design and fabrication of high-performance solar components with enhanced durability and efficiency. These developments pave the way for improved photoelectric conversion efficiency (PCE) and overall system performance, thereby enhancing the competitiveness and viability of solar energy as a mainstream energy source.

Central to the advancement of solar energy technology is the continuous refinement of solar cell designs and architectures [4]. Since the inception of photovoltaics in 1883, significant strides have been made in developing diverse photovoltaic structures tailored to specific applications and performance requirements. Silicon-based photovoltaics, renowned for their maturity and reliability, continue to dominate optical analysis and the solar market owing to their proven track record and widespread availability [4]. However, the quest for more cost-effective and versatile photovoltaic technologies has spurred the development of alternative approaches, such as dye-sensitized photovoltaics (DSPs) and perovskite solar cells.

Among these, DSPs have garnered significant attention for their unique combination of affordability, safety, vibrancy, and stability [5-10]. DSPs offer distinct advantages over traditional silicon-based photovoltaic structures, including lower manufacturing costs, enhanced flexibility, and compatibility with a wide range of substrates. Furthermore, DSPs demonstrate excellent performance under low light intensities and different illumination angles, making them particularly sensitive and well-suited for indoor and diffuse light conditions [11].

Since their initial discovery with the pioneering work of Michael Grätzel et al., in developing DSPs using titanium dioxide ($TiO_2$) in 1991 marked a significant milestone in the field of solar energy [12] and have garnered significant attention owing to their notable benefits, which include affordability, abundant raw materials, and a straightforward manufacturing process [13-17]. In this research, DSPs were successfully produced by utilizing a porous $TiO_2$ film as a photo anode, achieving a photovoltaic efficiency of 7% [12]. Subsequent studies on DSPs have yielded a record PCE of approximately 13% [18]. DSPs, considered third-generation solar cells, are composed of four primary components: a photo anode, dye, electrolyte, and counter electrode, with the photo anode coated on a transparent conductive oxide substrate.

Despite these advancements, the initial promise of DSPs, several challenges impede their widespread adoption and commercialization. Chief among these challenges is the lower-than-expected PCE and the use of scarce metals in DSP fabrication [19, 20] and certain challenges persist in optimizing the performance of DSPs, particularly in mitigating recombination reactions at the photo anode interface [21]. For instance, the porous structure of the $TiO_2$ photo anode is essential for dye absorption was facilitates electron flow and dye adherence thereby increasing surface area and dye molecule adhesion. However, this porous structure also allows electrolyte fluid to penetrate, can inadvertently promote increased recombination reactions at the $TiO_2$/dye/electrolyte interfaces, leading to reduced photovoltaic performance.

These limitations necessitate innovative approaches to enhance the efficiency and sustainability of DSPs while reducing their environmental footprint. Addressing this challenge involves intercepting recombination at the $TiO_2$/dye/electrolyte interfaces and requires a multifaceted approach, encompassing,

achieved through for optimization of the electrode materials the use of blocking layers, different electrolyte compositions, and device architectures to minimize recombination losses and maximize overall efficiency.

On the other hand, the presence of trap states within the $TiO_2$ film can significantly impact charge transport efficiency and contribute to charge recombination, which can undermine the performance of DSPs [22]. These limitations necessitate innovative approaches to enhance the efficiency and sustainability of DSPs while reducing their environmental footprint. Addressing this challenge involves intercepting recombination at the $TiO_2$/dye/electrolyte interfaces and requires a multifaceted approach, encompassing, achieved through for optimization of the electrode materials the use of blocking layers, different electrolyte compositions, and device architectures to minimize recombination losses and maximize overall efficiency.

To address the challenges faced in dye-sensitized photovoltaics (DSPs), researchers have implemented the hydrolysis of titanium tetrachloride (TiCl4) [23-27]. This method aims to modify the surface of mesoporous TiO2 films, enhancing the interaction between TiO2 nanoparticles. TiCl4 treatment involves adding an extra layer of TiO2, which results in larger particle sizes and improved dye adsorption on the DSP photo anode [28]. Subsequent heating of TiO2 films treated with TiCl4 converts TiCl4 solution components into TiO2 surface crystals. Studies have shown that TiCl4 treatment reduces gaps at the TiO2/perovskite interface, enhancing wettability and facilitating the deposition of perovskite precursor solutions [29].

Furthermore, $TiO_2$ crystals resulting from $TiCl_4$ treatment have demonstrated enhanced solar cell performance by modifying $TiO_2$ kinetic properties, affecting charge injection, transport, and recombination at appropriate conduction band edge positions [12, 30-32]. Murakami et al. [30] investigated the mechanism of TiCl4 treatment and demonstrated that it shifts the conduction band edge of the $TiO_2$ compact layer to higher energy levels, enhancing charge separation at the $TiO_2$/electrolyte interface and increasing photocurrent and overall performance.

Additionally, surface traps predominantly located on the $TiO_2$ surface contribute to charge recombination or impede charge transport [33]. $TiO_2$ surface crystals obtained from $TiCl_4$ hydrolysis have the potential to reduce interfacial trap density, thereby improving charge transport and reducing recombination after treatment [34, 35]. Studies have explored $TiCl_4$ treatment at lower temperatures (130 °C) to achieve a TiO2 coating with non-stoichiometric titanium dioxide, $TiO_x$, effectively mitigating surface traps and reducing surface roughness [36, 37].

In recent investigations, $TiCl_4$ treatment has been recognized as a promising strategy to optimize the performance of DSPs. By altering the $TiO_2$ film surface, $TiCl_4$ treatment enhances the overall efficiency and stability of DSP devices. The addition of an extra layer of TiO2 through $TiCl_4$ hydrolysis not only increases particle size but also promotes better dye adsorption, leading to improved light harvesting and photocurrent generation [28].

Moreover, the conversion of $TiCl_4$ solution species into TiO2 surface crystals via post-heating is critical for improving the interface properties of DSPs [29]. This treatment reduces gaps at the $TiO_2$/perovskite interface, facilitating the deposition of perovskite precursor solutions and enhancing the overall device performance [29].

The modifications induced by $TiCl_4$ treatment on $TiO_2$ crystals have profound effects on charge dynamics within DSPs. The altered kinetic properties of $TiO_2$, such as charge injection and transport, contribute to enhanced charge separation and reduced recombination, ultimately improving device efficiency [12, 30-32]. Murakami et al. [30] specifically demonstrated that $TiCl_4$ treatment shifts the conduction band edge of the $TiO_2$ compact layer to higher energy levels, which is advantageous for charge separation at the $TiO_2$/electrolyte interface.

Furthermore, $TiO_2$ surface crystals derived from $TiCl_4$ treatment play a crucial role in reducing interfacial trap density [34, 35]. This reduction in trap density improves charge transport efficiency and diminishes charge recombination, leading to higher overall device performance and stability. Lower-temperature $TiCl_4$ treatment has also been explored to achieve a TiO2 coating with non-stoichiometric titanium dioxide, effectively passivating surface traps and reducing surface roughness [36, 37]. These advancements underscore the significance of TiCl4 treatment as a versatile approach for enhancing the performance and stability of DSPs. In recent investigations, $TiCl_4$ treatment has been recognized as a promising strategy to

optimize the performance of DSPs. By altering the $TiO_2$ film surface, $TiCl_4$ treatment enhances the overall efficiency and stability of DSP devices. The addition of an extra layer of $TiO_2$ through $TiCl_4$ hydrolysis not only increases particle size but also promotes better dye adsorption, leading to improved light harvesting and photocurrent generation [28]. This approach addresses key challenges in DSPs related to charge transport, recombination, and interface properties, paving the way for more efficient and stable photovoltaic devices. These findings are particularly relevant for flexible substrates, where high temperatures required for crystalline $TiO_2$ coatings present limitations.

Open circuit voltage ($V_{OC}$) and photocurrent ($J_{SC}$) are significant parameters determining the PCE of a DSP. Regan et al. [33] applied $TiCl_4$ treatment onto TiO2-coated $SnO_2$ glass using a soaking technique, observing a 30–40% increase in $J_{SC}$ and a minor (3–7%) increase in fill factor (FF). The $V_{OC}$ largely remained unchanged, ultimately enhancing the PCE of the device through increased $J_{SC}$ rather than $V_{OC}$. Therefore, achieving a synergistic method that increases $V_{OC}$ while maintaining $J_{SC}$ is imperative. Similarly, Vesce et al. [38] proposed $TiCl_4$ pre- and post-treatments, resulting in increased $J_{SC}$ and PCE values compared to untreated samples. Research by Miranda-Gamboa et al. [39] indicated that $TiO_2$ films treated with $TiCl_4$ exhibited reduced oxygen vacancies and density of hydroxyl groups. Consequently, the device incorporating a $TiCl_4$-treated $TiO_2$ photo electrode achieved an enhanced power conversion efficiency (PCE) of 5.07% compared to that of pristine $TiO_2$ (4.57%).

In this study, two types of photovoltaic devices with planar architecture were fabricated using $TiO_2$ photo electrode layers treated with and without $TiCl_4$. The intrinsic performance of the $TiO_2$ films subjected to $TiCl_4$ treatment was systematically investigated.

Furthermore, it was noted that the efficiency of DSPs experiences a significant increase in low-light settings, with the $TiCl_4$-treated sample showing an efficiency boost from 22.4% to 27.5% under 0.1 $W/m^2$ conditions. This improvement underscores the effectiveness of $TiCl_4$ treatment in enhancing the performance of DSPs, particularly under challenging lighting conditions.

Additionally, the electrochemical properties of the DSPs were analyzed using Electrochemical Impedance Spectroscopy (EIS). This technique allowed for the characterization of key parameters such as electron lifetime, rise time, and fall time, which are crucial for understanding sensor behavior and performance. Notably, response times of approximately 4.1 nanoseconds for $TiCl_4$-treated DSPs and 5.3 nanoseconds for untreated DSPs were observed, highlighting the influence of $TiCl_4$ treatment on response speed.

In summary, this study demonstrates the significant potential of $TiCl_4$ treatment in enhancing the sensitivity and efficiency of DSPs, particularly in low-light conditions. By improving the device performance metrics such as efficiency and response time, $TiCl_4$ treatment offers valuable insights for optimizing DSP fabrication processes. These insights are crucial for advancing DSP technology and expanding its applications, especially in environments where reliable sensing capabilities under limited illumination are essential. The findings from this research contribute to the ongoing development and optimization of DSPs for various practical applications, including environmental monitoring and low-light sensing tasks.

## II. EXPERIMENTAL STUDY

### *A. Materials and DSP Fabrication*

Chemical reagents, vital for the experimentation, were meticulously sourced from Merck, while the chemical cleansing of substrates was carried out with precision using de-ionized water. Key materials, including Ti-Nanoxide D/SP Titania paste and FTO (Flor doped $SnO_2$ glass substrates (15 Ω/sq), were procured from Solaronix, ensuring the integrity and quality of the experimental setup. The fabrication process of $TiO_2$-based photo electrodes involved a meticulous application of Titanium paste onto fluoride doped indium tin oxide coated glass substrates (FTO) using the doctor blade technique, resulting in the formation of a uniform $TiO_2$ film with a thickness of approximately ~12 μm. In the course of the experiments, the control group was devoid of $TiCl_4$ treatment, while the experimental group underwent the application of $TiCl_4$ treatment as part of the protocol. These electrodes, each boasting a square active area

measuring 0.25 $cm^2$ (5x5 $mm^2$), were subjected to a rigorous sintering process at 500 ˚C for 30 minutes under controlled environmental conditions both before and after undergoing $TiCl_4$ treatment.

The utilization of $TiCl_4$, meticulously obtained from Sigma Aldrich, in a precisely calibrated 30 mM aqueous solution played a pivotal role in the enhancement of $TiO_2$ photo-electrodes. Post-treatment, the electrodes were subjected to a meticulous immersion process in a dye solution for 12 hours at room temperature in darkness, facilitating the incorporation of the N712 dye (cis-diisothiocyanato-bis(2,2'-bipyridyl-4,4'-dicarboxylato)ruthenium(II) tetrakis(tetrabutylammonium)), meticulously procured from Solaronix. This dye, prepared in an ethanolic solution at a concentration of 0.3 mM, ensured optimal light absorption and electron transfer properties, thus augmenting the overall efficiency of the photo electrodes.

Following the immersion process, meticulous ethanol rinsing was employed to remove any excess dye, after which the electrodes were meticulously dried to achieve their final configuration. The meticulous preparation of the electrolyte solution, in accordance with established protocols from a previous study [40], ensured consistency and reliability in the experimental setup. Platinum counter electrodes, meticulously fashioned on FTO-coated glass substrates using platinum paste from Sigma Aldrich, were meticulously heated to 420 ˚C for 15 minutes to ensure optimal conductivity and stability.

The meticulous assembly of the photo-electrodes and Pt counter electrodes using Meltonix 1170-60 hot-melt sealing film, sourced from Solaronix, facilitated a seamless integration, ensuring optimal electrolyte penetration and minimal leakage. To mitigate potential experimental discrepancies and ensure the reliability of the results, measurements were meticulously conducted using three independently prepared samples.

### *B. Characterization and Measurements*

The examination encompassed thorough scrutiny of the I-V measurements and photo detecting properties of all devices under varying conditions, including both dark and illuminated settings. Critical parameters such as $I_{SC}$, $V_{OC}$, FF, and μ%, indicative of the DSPs' performance characteristics, were meticulously evaluated in relation to irradiance intensity. Given the relative lack of emphasis on DSPs in low light environments, the establishment of a standardized laboratory illumination source replicating indoor lighting conditions remains elusive. Consequently, this study embarked on a comprehensive analysis, probing various characteristic parameters of the DSPs through a standardized irradiation test conducted at 1000 $W/m^2$ employing the Science Tech SLB-300A equipment. Furthermore, the evaluation of DSP parameters extended to encompassing different illumination intensities, spanning from 0.1 to 500 $W/m^2$ across twelve increments, meticulously executed within laboratory settings. This comprehensive assessment aimed to elucidate the DSPs' response across a spectrum of lighting conditions, providing valuable data for further analysis and optimization.

In addition to the I-V measurements and photo detecting properties analysis, the Electrochemical Impedance Spectroscopy (EIS) of the produced DSPs was meticulously conducted. Under AM 1.5-1000 $W/m^2$ illumination, the EIS analysis was performed at room temperature within a Faraday cage utilizing a Gamry ref. 600 potentiostat/galvanostat. The application of a 10 mV amplitude AC oscillator signal facilitated the comprehensive exploration of frequency responses ranging from 10 mHz to 1 MHz at a bias of -0.6 V for all samples during dark tests. Subsequently, the Nyquist plots of the DSPs were fitted to the equivalent circuit, providing valuable insights into their electrochemical behavior. The Nyquist plots of DSPs were fitted to the equivalent circuit illustrated in Figure 1.

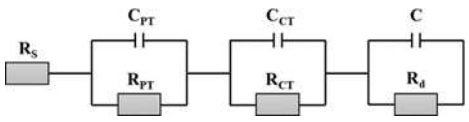


Figure 1. The employed equivalent circuit for fitting the parameters of the DSP. Equivalent circuit model of the DSPs in which $R_S$: serial resistance of FTO glass, $C_{PT}//R_{PT}$: impedance at the counter electrode/electrolyte interface, $C_{CT}//R_{CT}$: impedance at $TiO_2$/dye/ electrolyte interface and $C//R_d$: impedance due to the diffusion process of $I^-/I_3^-$ redox couple in the electrolyte ($Z_w$) [41, 42].

The determination of series resistance ($R_S$), extracted from the Nyquist curves within the equivalent circuit, is crucial for understanding the impedance behavior of DSPs. $R_S$ represents the resistance associated with the FTO layer, discerned by identifying the curve's origin point. The Nyquist curves, characteristic of impedance spectroscopy analysis, display distinct kinetic loops across low, mid, and high-frequency regions. Notably, the initial loop observed in the high-frequency domain reflects the resistance attributed to the charge transfer process at the Pt counter electrode-electrolyte interface ($R_{PT}$) [43]. Additionally, the second resistance parameter, $R_{CT}$, discerned from the expansive loop within the mid-frequency domain, characterizes the charge transfer resistance at the $TiO_2$/dye/electrolyte interfaces [44].

An investigative approach was adopted to comprehensively assess the response time of DSP devices under specified test conditions. Transient photo voltage and transient photocurrent measurements were meticulously conducted, with dye-sensitized samples stimulated by a 660 nm wavelength pulse. The pulse, featuring a period of 1 second and a pulse width of 200 ms, facilitated detailed time response analysis. It is well-established in literature that a pulse frequency of 1 Hz is deemed sufficiently low and conducive for capturing the complete signal amplitude in time response analysis [45].

The configuration of illumination sources played a pivotal role in ensuring accurate and consistent measurements. Light emitting diodes were meticulously chosen to provide optical power outputs of 0.0974 $mW/cm^2$ for red light and 1.39 $mW/cm^2$ for white light. These optical power measurements were conducted using a precise laser power meter (Newport 818-R) to ensure reliability and reproducibility. Following the acquisition of experimental I-V characteristics of the DSP devices were meticulously computed based on the device's response to red light signals at a wavelength of 660 nm. The monochromatic light was modulated to ensure accurate measurements, accompanied by continuous bias irradiation to maintain stability and consistency. Notably, simultaneous measurements were conducted to capture the device's response under varying conditions accurately.

In addition, electron lifetime ($\tau_e$) and electron transport time ($\tau_{trans}$) values were calculated by using the parameters in the Bode plots of DSPs that $f_{max}$ and chemical capacitance ($C_{CT}$) values by using the equations (1) and (2) given below, and these values were collected in a table. Nyquist plots of DSPs were obtained and presented which were used to examine the time constants of the DSPs.

$$\boldsymbol{\tau_e} = \frac{1}{2\pi f_{max}} \tag{1}$$

$$\boldsymbol{\tau_{trans}} = R_{CT}.C_{\mathbf{CT}} \tag{2}$$

where, $f_{max}$ is the peak frequency value that obtained from the Bode plot of DSP, $R_{CT}$ and $C_{CT}$ are obtained from Nyquist plot [46].

## III. Experimental Results

In this investigation, the study focused on evaluating the influence of TiCl4 treatment on the response and detection parameters of DSPs under low-light conditions. Electrical measurements were conducted across a range of illumination levels, including standard conditions and gradually reduced low-light settings spanning 13 steps from 1000 W/m2 down to 0.1 W/m2.

To assess the individual I-V characteristics of each DSP, experiments were initiated with AM 1.5, 1000 W/m2 illumination measurements. Notably, the DSP treated with TiCl4 exhibited superior performance compared to untreated devices. Despite conducting measurements under identical conditions, variations in short-circuit currents, voltages, fill factors, and other parameters were observed between the two types of DSPs due to differences in their manufacturing processes. These differences directly influence the power output and overall performance of the cells.

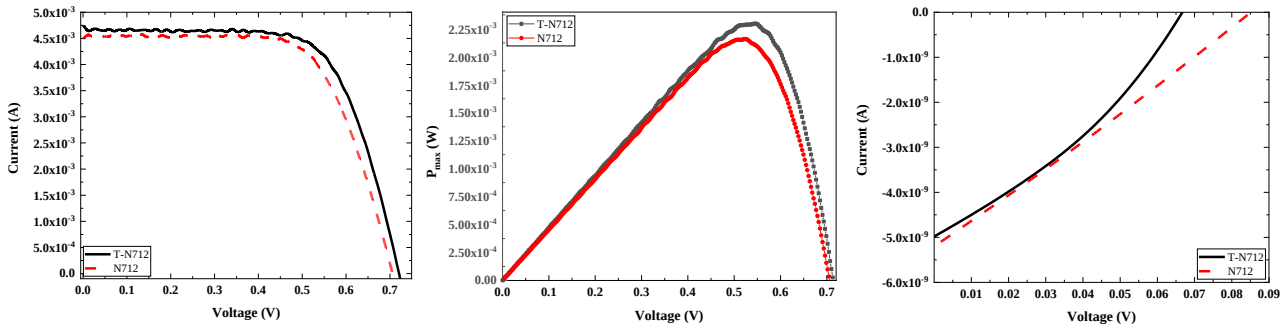


Figure 2. I–V measurements and the power outputs of the DSPs under AM 1.5, 1000 W/m$^2$ illumination.

Figure 2 presents the efficiency performance of the individual DSPs. Figure 2 (a) depicts the independently determined I-V curves of all DSPs under white light, while Figure 2 (b) presents the corresponding power outputs. The study highlights that T-N712 exhibited a maximum efficiency of 9.33%, surpassing N712, which achieved 8.13%. The parameters were calculated as [46]. These results underscore significant advancements in dye-sensitized photovoltaic technology, demonstrating the effectiveness of $TiCl_4$ treatment in enhancing device efficiency. The findings suggest promising prospects for further optimizing DSPs and advancing their performance in photovoltaic applications. The $TiCl_4$ treated T-N712 demonstrated the highest power output at 2.3 mW, slightly outperforming the untreated N712, which achieved an output of 2.1 mW under white illumination conditions. This improvement is primarily attributed to the reduction in interfacial trap density at the $TiO_2$/dye/electrode interface with $TiCl_4$ treatment [39].

Despite the linear behavior observed in the I-V plots of Figure 2 (c) for DSPs under dark conditions, the I-V curves shown in Figure 2 (a)-(c) exhibit nonlinearity and rectifying characteristics, indicative of photovoltaic properties. Both devices display short-circuit currents of approximately 0.005 μA and built-in potentials of 0.06 V and approximately 0.085 V for T-N712 and N712, respectively. The built-in potential in these devices is a result of junction formation at the electrolyte-$TiO_2$ interface and ohmic contact with the electrodes, facilitating the separation of electron-hole pairs generated by light. This inherent potential enables photocurrent generation without bias voltage and supports self-powered operation under illumination. The observed weak built-in potential is mainly due to the ohmic contact between electrodes and electrolyte, causing photo-excited carriers in the $TiO_2$ to move outward, generating external photocurrent without requiring external power. This mechanism underscores the importance of interface properties in enhancing photovoltaic performance. This phenomenon underscores the intrinsic photovoltaic behavior of the DSPs, where light-induced charge carriers contribute to the creation of a photovoltaic effect even in the absence of an applied bias. The observed rectification behavior and built-in potential highlight the semiconductor properties of the $TiO_2$ material in the DSPs, which facilitate efficient charge separation and transport essential for photovoltaic operation. These findings illustrate the unique characteristics of DSPs, emphasizing their suitability for self-powered applications leveraging ambient light sources for energy conversion.

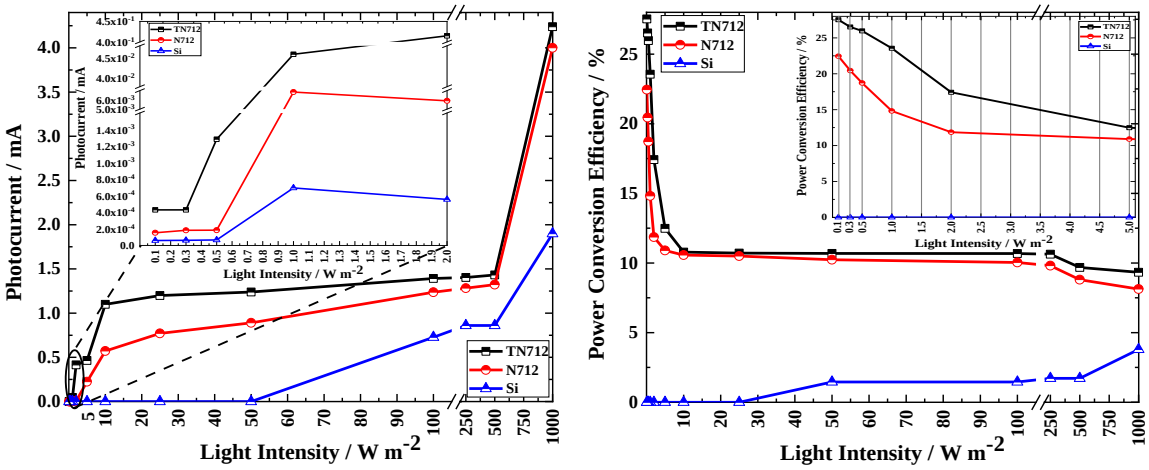


Figure 3. Photocurrent measurements (a) and Power Conversion Efficiencies (b) of the DSPs and c-Si sensor, based on the various light intensities that were ranging as 1000, 500, 250, 100, 50, 25, 10, 5, 2, 1, 0.5, 0.3 and 0.1 W/m$^2$ respectively (insets: measurements in the 5 W/m2 and lower illumination levels)

Figure 3 provides a comparative analysis between c-Si and DSPs. The figure presents the measured photocurrent and PCE curves for both c-Si photodetectors and DSPs. The experimental setup involved electrical measurements conducted under various illumination conditions, systematically decreasing across 13 steps as 1000, 500, 250, 100, 50, 25, 10, 5, 2, 1, 0,5, 0,3 and 0,1 W/m$^2$.

Comparing the $I_{SC}$ values in Figure 3 (a), both $TiCl_4$-treated and untreated DSPs exhibit nearly identical current levels, slightly higher than those observed with the Si photodetector. Despite the slightly higher photo voltage from the Si photodetector, DSPs demonstrate more stable PCE characteristics and greater sensitivity to changes in overall illumination levels as shown in Figure 3 (b).

At these reduced lighting intensities, the c-Si photodetector's energy conversion efficiency remains lower and relatively stable, indicating challenges in responding to light levels rather than light quantity. The graphs clearly depict that DSP performance is less impacted by lower light conditions compared to the c-Si sensor, highlighting DSPs' sensitivity and adaptability to varying light conditions.

The distinct responses of DSPs to each step of light intensity change under similar conditions underscore their stable transfer characteristics, closely approximating the ideal theoretical behavior expected from photovoltaic devices.

Additionally, electrochemical properties were investigated using EIS analysis to assess parameters such as series and parallel resistance values and electron lifetime. Additionally, photodetector parameters such as rise time, and fall time were obtained for comprehensive characterization and comparison of the DSPs. To assess the impact of $TiCl_4$ treatment on charge transport properties of $TiO_2$ photo anodes and subsequent DSPs, Electrochemical Impedance Spectroscopy (EIS) was conducted with a perturbed voltage of 0.6 V. Figure 4 depicts EIS Nyquist plots for all DSP devices exposed to 100 mW/cm$^2$ irradiance, with corresponding parameters detailed in Table 1. This analysis provides valuable insights into how $TiCl_4$ treatment influences impedance responses and charge transport dynamics within photo anodes, critical for optimizing DSP performance.

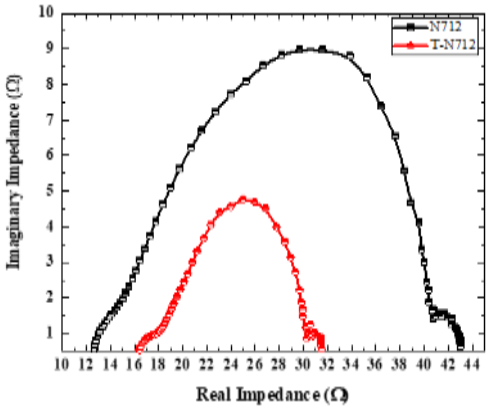


Figure 4. The generated EIS Nyquist diagrams for DSPs employing $TiO_2$ films treated with and without $TiCl_4$.

In the analysis of dye-sensitized solar cells (DSPs), the internal resistance ($R_S$) associated with the electrical contacts and the $I^-/I_3^-$ electrolyte is typically determined by examining the intercept on the real axis in the high-frequency region of the Nyquist plot [47]. This plot consists of three distinct arcs, each revealing different aspects of the cell's behavior and providing valuable insights into its performance characteristics.

The first arc observed on the Nyquist plot, progressing from left to right, corresponds to the diffusion resistance at the interface between the $I^-/I_3^-$ electrolyte and the Pt counter electrode [48]. This arc offers critical information about the ionic transport processes occurring at this junction, which significantly influence the overall performance and efficiency of the cell.

The second arc on the Nyquist plot represents the charge transport resistance ($R_{CT}$) at the interface between the $TiO_2$ photo anode, electrolyte, and counter electrode in the mid-frequency range [48]. Analysis of this arc provides key insights into charge transfer kinetics and electron transport properties within the photo anode and electrolyte, essential for optimizing cell efficiency.

Moving from right to left, the third arc in the Nyquist plot signifies the charge transport resistance ($R_{PT}$) at the interface between the electrolyte and Pt electrode [48]. This arc allows for a detailed examination of charge transfer processes at this interface, contributing to a comprehensive understanding of factors influencing the overall performance and behavior of DSPs.

The Nyquist plot and analysis of its arcs serve as powerful tools for studying and optimizing DSPs. By deciphering the resistances and processes represented by each arc, researchers can identify areas for improvement and refine the design of DSPs to enhance their efficiency and performance in converting solar energy into electrical energy [48].

The EIS results presented in Figure 4 and Table 1 demonstrate the impact of $TiCl_4$ treatment on the impedance characteristics of DSP devices.

Notably, $TiCl_4$-treated photo anodes exhibit altered impedance profiles compared to untreated counterparts, indicating improved charge transport and reduced internal resistances at key interfaces within the DSP structure.

Table 1. The DSPs' measured parameters Equivalent circuit parameters of the DSSCs according to electrochemical impedance spectroscopy

| Dye | Parameters | Value |
|---|---|---|
| N712 | $V_{OC}$ (mV) | 711 |
| | $J_{SC}$ (mA/cm$^2$) | 22 |
| | FF | 0,520 |
| | **η (%)** | **8,134** |
| | $I_{dark}$ (mA) | 5.16 x $10^{-6}$ |
| | Rs (error %) | 15,63 (1,19) |
| | $R_{PT}$ (error %) | 6,45 (7,22) |
| | $C_{PT}$ (error %) | 2,02 x$10^{-5}$ |
| | $R_{CT}$ (error %) | 7,81 (8,05) |
| | $C_{CT}$ (error %) | 2,19x$10^{-4}$ |
| | $R_d$ (error %) | 0,45 (3,11) |
| | C (error %) | 0,49 |
| | ($\tau_e$) (ms) | 37 |
| | ($\tau_{trans}$)(ms) | 73 |
| | Response Time (ns) | 5,3 |
| | Response Rate (mV) | 2,1 |
| | Fall Time (ms) | 103 |
| T-N712 | $V_{OC}$ (mV) | 719 |
| | $J_{SC}$ (mA/cm$^2$) | 23,5 |
| | FF | 0,552 |
| | **η (%)** | **9,328** |
| | $I_{dark}$ (mA) | 4.9096 x $10^{-6}$ |
| | Rs (error %) | 12,64 (1,08) |
| | $R_{PT}$ (error %) | 5,72 (8,25) |
| | $C_{PT}$ (error %) | 1,22 x$10^{-5}$ |
| | $R_{CT}$ (error %) | 24,08 (5,11) |
| | $C_{CT}$ (error %) | 3,02 x$10^{-4}$ |
| | $R_d$ (error %) | 2,14 (5,76) |
| | C (error %) | 0,24 |
| | ($\tau_e$) (ms) | 46 |
| | ($\tau_{trans}$)(ms) | 94 |
| | Response Time (ns) | 4,1 |
| | Response Rate (mV) | 2,9 |
| | Fall Time (ms) | 81 |

The data presented in Table 1 reveals an intriguing relationship between the charge transport resistance ($R_{PT}$) at the Pt-electrolyte interface and the observed short-circuit currents in dye-sensitized solar cells (DSPs), suggesting a potential correlation with the concentration of triiodide ions ($I_3^-$) ions in the electrolyte. To enhance efficient dye regeneration in electrodes with higher photocurrent densities, facilitating the oxidation of $I^-$ ions to $I_3^-$ is crucial, increasing the $I_3^-$ ion concentration in the electrolyte. Previous studies have established a direct link between the reciprocal of the charge-transfer resistance at the platinum/electrolyte interface and the square root of the concentration of $I_3^-$ in the electrolyte [43].

Optimizing charge transfer dynamics at the Pt-electrolyte interface is key to promoting effective dye regeneration and improving overall cell performance. By increasing $I_3^-$ ion concentration through controlled oxidation processes, charge transport limitations can be mitigated, enhancing electron transfer efficiency in dye-sensitized solar cell architecture. Understanding these relationships allows for targeted strategies in electrode design and electrolyte composition, optimizing charge transport properties to improve the performance and stability of dye-sensitized solar cells.

The observed inverse relationship between $R_{PT}$ and short-circuit currents underscores the importance of optimizing $I^-$ oxidation to enhance DSP performance. By increasing the concentration of $I_3^-$ ions through oxidation, the electrolyte can support efficient dye regeneration, ultimately contributing to improved charge transport and overall device efficiency. This understanding of ion concentration dynamics at the electrode-electrolyte interface is crucial for advancing the design and performance of DSPs. The reciprocal relationship between charge-transfer resistance and $I_3^-$ concentration serves as a valuable guide for optimizing electrolyte compositions and electrochemical processes in DSSC technologies.

The observed inverse relationship between $R_{PT}$ and short-circuit currents suggests that variations in $I_3^-$ concentration impact charge transport properties within the DSP system. Higher $I_3^-$ concentrations facilitate more efficient dye regeneration, resulting in increased photocurrents. This phenomenon underscores the importance of electrolyte composition in optimizing the performance of dye-sensitized photovoltaics, particularly in relation to charge transfer kinetics at the electrode/electrolyte interface.

The relationship between $R_{PT}$ and short-circuit currents highlights the dynamic interplay between electrolyte composition and device performance in DSPs. By manipulating $I_3^-$ concentrations through controlled oxidation processes, researchers can fine-tune charge transport properties to enhance overall efficiency and stability. This understanding contributes to the ongoing optimization of DSP technology for renewable energy applications.

Furthermore, the data presented in Figure 4 underscores a substantial distinction in the size of the primary semicircle evident in all $TiCl_4$-treated DSPs compared to the untreated counterpart. This difference signifies the significant impact of $TiCl_4$ in mitigating recombination at the oxide/electrolyte interface. The observed effect is attributed to the formation of a protective layer at the $TiO_2$/electrolyte junction, which reduces recombination rates and enhances the performance and efficiency of treated DSPs compared to untreated ones. This controlled modification by $TiCl_4$ improves charge transport characteristics and reduces recombination losses at the interface.

The larger semicircle in the Nyquist plot for $TiCl_4$-treated DSPs suggests lower charge transfer resistance at the interfaces, highlighting improved electron transport properties. This protective layer likely enhances charge separation and reduces charge recombination, leading to more efficient electron collection and improved device performance. The findings highlight the beneficial impact of $TiCl_4$ treatment on DSPs, showcasing its potential to boost device efficiency and stability in practical applications.

The protective layer generated by $TiCl_4$ acts as a barrier, reducing charge carrier losses at the interface and enhancing charge transport properties within the photovoltaic device. These findings underscore the importance of $TiCl_4$ treatment in optimizing DSP performance and highlight its role in mitigating recombination losses, thereby contributing to the overall efficiency enhancement of dye-sensitized photovoltaics.

Determining the electron mean lifetime ($\tau_e$) in these devices is essential for understanding their performance characteristics as shown in Table 1. The electron mean lifetime represents the duration that an excited electron remains in a conduction state before returning to its valence band state due to recombination processes. The determination of this parameter involves analyzing the peak frequency value ($f_{max}$) from the Bode plot obtained from EIS, corresponding to the peak of the $R_{CT}$ arc [46]. This frequency value reflects critical charge transfer kinetics within the photovoltaic system.

The electron mean lifetime ($\tau_e$) is calculated based on the described method [46]. For the bare electrode, $\tau$ is found to be 37 ms, whereas for the $TiCl_4$-treated electrodes, $\tau$ is extended to 46 ms. These values are consistent with previously reported data for similar dye-sensitized photovoltaic systems [46]. The observed improvement in $\tau$ with $TiCl_4$ treatment can be attributed to enhanced diffusion length and reduced recombination rates [49].

Comparatively higher $\tau_e$ values with $TiCl_4$ treatment signify that devices with $TiCl_4$-treated electrodes achieve a lifetime performance exceeding 24% of their bare counterparts. This finding underscores the significance of $TiCl_4$ treatment as a key optimization strategy for dye-sensitized photovoltaic devices.

The electron mean lifetime ($\tau_e$) serves as a crucial indicator of the charge carrier dynamics within the electrodes and interfaces of dye-sensitized photovoltaics. A longer $\tau_e$ indicates a reduced rate of charge recombination, contributing to enhanced device performance and efficiency. By optimizing $\tau_e$ through $TiCl_4$ treatment, these devices exhibit improved charge transport properties and reduced losses, leading to higher overall performance under operational conditions [49]. Thus, $TiCl_4$ treatment is a valuable approach to enhance the electron mean lifetime ($\tau_e$) and optimize the performance of dye-sensitized photovoltaic devices.

Remarkably, the influence of $TiCl_4$ treatment was particularly pronounced under low illumination levels. DSPs treated with $TiCl_4$ exhibited a remarkable increase in short-circuit current density ($J_{SC}$) by over 6.3% compared to DSPs with bare $TiO_2$ at various levels of illuminance. This enhancement in $J_{SC}$ suggests that

$TiCl_4$ treatment enhances the light-harvesting ability of the DSPs, likely due to improved dye loading and charge extraction efficiency at lower light intensities.

Furthermore, the change in open-circuit voltage ($V_{OC}$) with decreasing illuminance was more gradual for DSPs treated with $TiCl_4$. This observation indicates that $TiCl_4$ treatment helps maintain a stable $V_{OC}$ across different light conditions, which is critical for achieving consistent performance in varying environments.

In addition, the fill factor (FF) of DSPs treated with $TiCl_4$ displayed an increasing trend as illuminance decreased, contrasting with the FF of bare $TiO_2$, which typically decreases under lower light levels. The improved FF with $TiCl_4$ treatment suggests enhanced charge transport and reduced losses within the device, contributing to overall improved performance.

These results underscore the effectiveness of $TiCl_4$ treatment in suppressing electron-hole recombination within the DSPs, especially under conditions of reduced illumination. By reducing recombination, $TiCl_4$ treatment improves the overall efficiency and stability of DSPs in indoor lighting environments, where light levels are typically lower compared to outdoor settings.

Overall, the integration of $TiCl_4$ treatment into DSPs leads to enhancements in $J_{SC}$ and FF under standard AM 1.5 conditions, ultimately resulting in improved power conversion efficiency (PCE). At an illuminance of 0.1 $W/m^2$, the PCE of $TiCl_4$-treated DSPs increases to 27.5%, compared to 22.4% for untreated DSPs. This represents a significant 22.8% increase in PCE facilitated by $TiCl_4$ treatment under low-light conditions, highlighting its potential to optimize the performance of DSPs across a range of lighting scenarios.

Additionally, our study delved into analyzing the photodetector characteristics of DSPs using the N712 dye as the photosensitizer. We conducted a comprehensive assessment of DSPs' photodetector applications by examining their response times for photo responsivity through transient photo current and photo voltage measurements. This evaluation aimed to understand how DSPs perform as photodetectors, providing insights into their responsiveness and suitability for practical photo detection applications. The performance of DSPs are intricately linked to the characteristics of the dyes utilized and the structural composition of the $TiO_2$ layer within the devices [50]. Hence, within the scope of my research, we identified $TiCl_4$ treatment as a viable strategy for enhancing the photo activity of DSP photo electrodes.

Additionally, my observations revealed that DSP photodetectors exhibited an initial surge in current within the first few nanoseconds of exposure to light, transitioning to a sustained current generation approximately around ~0.1 seconds thereafter as shown in Figures 5 and 6. This temporal delay in current generation was attributed to the duration of redox reactions within the photochemical cell, catalytic processes, and the rate of electron transport within the liquid electrolyte.

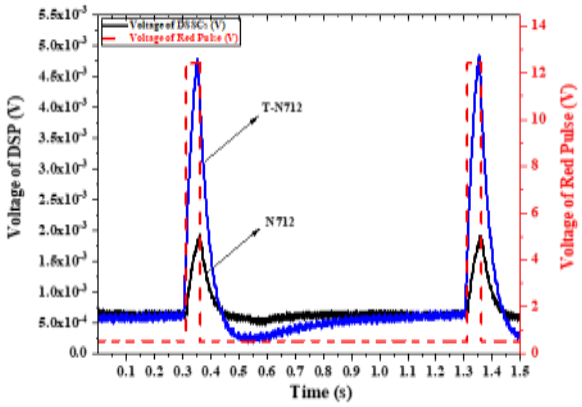


Figure 5. Photovoltage vs. Time responses of the DSPs for red light pulse.

During red pulse illumination, the devices demonstrated a significant contrast ratio at zero bias, with the T-712 model exhibiting a contrast ratio 1.1 times higher than the N712 model, determined by the ratio of photo-current ($I_{ph}$) to dark current ($I_{Dark}$) [51, 52]. This observation highlights the efficacy of our custom devices for self-powered applications, leveraging ambient energy sources due to their photovoltaic effect,

high contrast ratio at zero bias, and suitable rectification ratio. However, the T-N712 device stands out with superior conversion efficiency, positioning it as a more favorable candidate for such applications.

To delve deeper into the origin of the self-powered response exhibited by these devices, we conducted measurements of their photo-voltage values under red pulse illumination. Figures 5 and 6 present the reproducible photo-voltage versus time for N712 and T-N712, respectively, generated by periodically switching the red pulse light on and off with a wavelength of 660 nm at 0 V bias.

The contrast ratio, a crucial parameter for self-powered applications, quantifies a device's effectiveness in converting light into electrical signals. The higher contrast ratio of the T-712 model compared to N712 indicates better performance under red pulse illumination, emphasizing the importance of device design and material composition. The presence of the photovoltaic effect, where incident light generates a voltage difference in the absence of an external bias, is evident from the photo-voltage measurements.

Moreover, the reproducibility of the photo voltage measurements demonstrates the stability and reliability of the devices under red pulse illumination, providing insights into charge carrier dynamics and material properties essential for optimizing these devices for practical applications.

In Figure 5, upon activation of red pulse irradiation at a power density of 0.0974 mW/cm$^2$, the T-N712 exhibited a notable jump of 4.8 mV in photo-voltage, compared to 1.9 mV observed for N712. This difference underscores the enhanced response of the $TiCl_4$-treated device to the red pulse illumination, attributed to improved charge carrier dynamics and reduced recombination processes.

Figure 6 illustrates the behavior of photo-voltage over time, showing that both devices reach maximum photo-voltage levels within nanoseconds after the pulse onset. Subsequently, a gradual reduction in photo-voltage occurs, indicative of current leakage due to minority carrier diffusion and electron-hole recombination. This dynamic behavior provides valuable insights into the operational characteristics of our devices under red pulse illumination, emphasizing the importance of optimizing charge transport and recombination processes for enhancing self-powered performance.

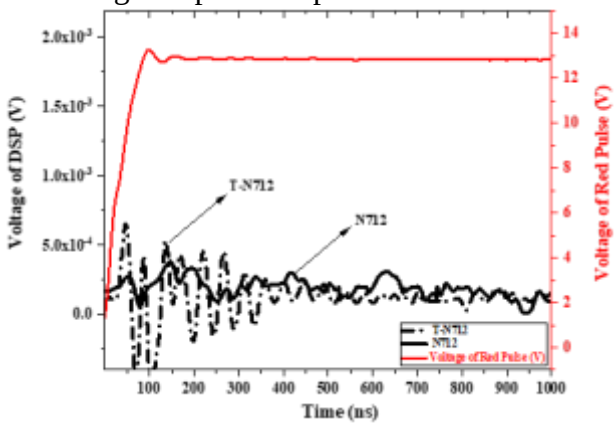


Figure 6. Impression of the rise time grown of the DSPs.

This comparative analysis underscores the significant impact of $TiCl_4$ treatment in enhancing the performance of DSPs under varying light intensities. The observed improvements highlight the potential of $TiCl_4$ treatment to optimize photodetector functionality and efficiency, particularly in low-light environments where sensitivity and responsiveness are critical. By systematically evaluating response and detection parameters across a range of illumination levels, this study provides valuable insights into the practical application and performance optimization of DSPs for diverse sensing and detection applications. Future research may further explore the underlying mechanisms driving these enhancements and seek to refine DSP fabrication processes to maximize their effectiveness under challenging lighting conditions.

## IV. CONCLUSIONS

This study delved into the intricate role played by N712 dye and $TiCl_4$ treatment in augmenting the performance of DSPs under conditions of low light. Our investigation underscored the considerable enhancement in DSP functionality resulting from $TiCl_4$ treatment, which translated to improved PCE when

compared to untreated cells under standard AM 1.5 illumination conditions. EIS analysis provides valuable insights into the charge transport behavior of DSPs with $TiCl_4$-treated and untreated $TiO_2$ photo anodes. The observed changes in impedance parameters highlight the effectiveness of $TiCl_4$ treatment in enhancing charge transfer kinetics and optimizing the overall performance of dye-sensitized photovoltaics.

The efficacy of $TiCl_4$ treatment in optimizing DSP performance was particularly evident when subjected to a spectrum of decreasing light intensities across 13 incremental steps ranging from 1000 to 0.1 $W/m^2$. The low light response exhibited a remarkable enhancement from 22.4% to 27.5% under 0.1 $W/m^2$, which is a fairly low illumination level, highlighting the superior capability of TiCl4 treatment support to DSPs in capturing and converting low light into electrical energy. The stability and sensitivity demonstrated by DSPs in response to varying light conditions underscore their potential for practical applications where light levels may fluctuate or be limited. This also underscores the potential of $TiCl_4$ treatment to bolster power generation even in environments characterized by low levels of illumination. These findings suggest that DSPs have a more robust and consistent performance profile under challenging low-light conditions compared to traditional silicon-based photodetectors.

Further optimization and refinement of DSP technology could lead to enhanced efficiency and reliability in real-world photovoltaic applications.

The implications of these findings extend significantly towards the development and optimization of DSPs for practical applications. As such, we envisage further research endeavors focusing on optical investigations as integral components of our future research trajectory. These future explorations will seek to elucidate and optimize the intricate interplay between $TiCl_4$ treatment, dye properties, and device structure, thereby advancing the performance and applicability of DSPs across a diverse array of real-world scenarios. Such efforts hold immense promise in furthering our understanding of DSPs and unlocking their full potential as versatile and efficient photo detection platforms in various applications, including sensing, imaging, and energy harvesting.

In conclusion, by embracing innovative approaches and harnessing the power of nanotechnology, researchers and engineers can overcome existing barriers.

## REFERENCES


[1] O. Jogunola, C. Morley, I. J. Akpan, Y. Tsado, B. Adebisi and L. Yao, Energy consumption in commercial buildings in a post-COVID-19 world, IEEE Eng. Manag. Rev., 2022. 50 (1), pp. 54-64, 1st Quart..

[2] L. Li, J. Lin, N. Wu, S. Xie, C. Meng, Y. Zheng, et al., Review and outlook on the international renewable energy development, Energy Built Environ., 2022. 3 (2), pp. 139-157.

[3] G. Li, M. Li, R. Taylor, Y. Hao, G. Besagni and C. N. Markides, Solar energy utilisation: Current status and roll-out potential, Appl. Thermal Eng., 2022. 209.

[4] S. A. Olaleru, J. K. Kirui, D. Wamwangi, K. T. Roro and B. Mwakikunga, Perovskite solar cells: The new epoch in photovoltaics, Sol. Energy, 2020. 196, pp. 295-309.

[5] O. I. Francis and A. Ikenna, Review of dye-sensitized solar cell (DSSCs) development, Natural Sci., 2021. 13(12), pp. 496–509.

[6] J. Yan, T. J. Savenije, L. Mazzarella, and O. Isabella, Progress and challenges on scaling up of perovskite solar cell technology, Sustain. Energy Fuels, 2022. 6 (2), pp. 243–266.

[7] P. Semalti and S. N. Sharma, Dye sensitized solar cells (DSSCs) electrolytes and natural photo-sensitizers: A review, J. Nanosci. Nanotechnol.,2020. 20(6), pp. 3647–3658.

[8] S. De Sousa, S. Lyu, L. Ducasse, T. Toupance, and C. Olivier, Tuning isible-light absorption properties of Ru-diacetylide complexes: Simple access to colorful efficient dyes for DSSCs, J. Mater. Chem. A, 2015. 3(35), pp. 18256–18264.

[9] X. Xie, Y. Zhang, Y. Ren, L. He, Y. Yuan, J. Zhang, and P. Wang, Semitransparent dye-sensitized solar cell with 11% efficiency and photothermal stability, J. Phys. Chem. C, 2022. 126(27), pp. 11007–11015.

[10] S. Yun, P. D. Lund, and A. Hinsch, Stability assessment of alternative platinum free counter electrodes for dye-sensitized solar cells, Energy Environ. Sci., 2015. 8(12), pp. 3495–3514.

[11] U. Mehmood, A. Al-Ahmed, F. A. Al-Sulaiman, M. I. Malik, F. Shehzad, and A. U. H. Khan, Effect of temperature on the photovoltaic performance and stability of solid-state dye-sensitized solar cells: A review, Renew. Sustain. Energy Rev., 2017. 79, pp. 946–959.

[12] B. O'Regan and M. Grätzel, A low-cost, high-efficiency solar cell based on dye-sensitized colloidal TiO2 films, Nature, 1991. 353(6346), pp. 737–740.

[13] P.R. Schol, W.S. Zhang, T. Scharl, A. Kunzmann, W. Peukert, R.R. Schröder, D.M. Guldi, Intrinsic and extrinsic incorporation of indium and single-walled carbon nanotubes for improved ZnO-based DSSCs. Adv. Energy Mater. 2022. 12(13), 2103662.
[14] K.S. Keremane, A. Planchat, Y. Pellegrin, D. Jacquemin, F. Odobel, A.V. Adhikari, Push-pull phenoxazine-based sensitizers for p-type DSSCs: Effect of acceptor units on photovoltaic performance. Chem. Sustain. Energy Mater. 2022. 15, 1–14.
A. Atli, A. Atilgan, C. Altinkaya, K. Ozel, A. Yildiz, St. Lucie cherry, yellow jasmine, and madder berries as novel natural sensitizers for dye-sensitized solar cells. Int. J. Energy Res. 2019. 43(8), 3914–3922.
B. Atilgan, A. Yildiz, Ni-doped TiO2/TiO2 homojunction photoanodes for efficient dye-sensitized solar cells. Int. J. Energy Res. 2022. 46, 14558.
[15] Y. Kocak, A. Atli, A. Atilgan, A. Yildiz, Extraction method dependent performance of bio-based dye-sensitized solar cells (DSSCs). Mater. Res. Express. 2019. 6(9), 095512.
[16] J. Burschka, N. Pellet, S.J. Moon, R. Humphry-Baker, P. Gao, M.K. Nazeeruddin, M. Grätzel, Sequential deposition as a route to high-performance perovskite-sensitized solar cells. Nature 2013. 499(7458), 316–319.
[17] M. Graetzel, R. A. J. Janssen, D. B. Mitzi, and E. H. Sargent, Materials interface engineering for solution-processed photovoltaics, Nature, 2012. vol. 488(7411), pp. 304–312.
[18] M. Younas, M. A. Gondal, M. A. Dastageer, and K. Harrabi, Efficient and cost-effective dye-sensitized solar cells using MWCNT-TiO2 nanocomposite as photoanode and MWCNT as Pt-free counter electrode, Sol. Energy, 2019. 188, pp. 1178–1188.
[19] M. Filipič, M. Berginc, F. Smole, and M. Topič, Analysis of electron recombination in dye-sensitized solar cell, Current Appl. Phys.,2012. 12(1), pp. 238–246.
[20] Zhu, K., Kopidakis, N., Neale, N. R., Van De Lagemaat, J., & Frank, A. J. Influence of surface area on charge transport and recombination in dye-sensitized TiO2 solar cells. The Journal of Physical Chemistry B, 2006. 110(50), 25174-25180.
[21] Lee, S. W., Ahn, K. S., Zhu, K., Neale, N. R., & Frank, A. J. Effects of TiCl4 treatment of nanoporous TiO2 films on morphology, light harvesting, and charge-carrier dynamics in dye-sensitized solar cells. The Journal of Physical Chemistry C, 2012. 116(40), 21285-21290.
[22] Marchioro, A., Dualeh, A., Punzi, A., Grätzel, M., & Moser, J. E.. Effect of posttreatment of titania mesoscopic films by TiCl4 in solid-state dye-sensitized solar cells: a time-resolved spectroscopy study. The Journal of Physical Chemistry C, 2012. 116(51), 26721-26727.
[23] Adhikari, S. G., Shamsaldeen, A., & Andersson, G. G. The effect of TiCl4 treatment on the performance of dye-sensitized solar cells. The Journal of Chemical Physics, 2019. 151(16), 16470.
[24] Ostapchenko, V., Huang, Q., Zhang, Q., & Zhao, C. Effect of TiCl4 treatment on different TiO2 blocking layer deposition methods. International Journal of Electrochemical Science, 2017. 12(3), 2262-2271.
[25] Choi, H., Nahm, C., Kim, J., Moon, J., Nam, S., Jung, D. R., & Park, B. The effect of TiCl4-treated TiO2 compact layer on the performance of dye-sensitized solar cell. Current Applied Physics, 2012. 12(3), 737-741.
[26] Sommeling, P. M., O'Regan, B. C., Haswell, R. R., Smit, H. J. P., Bakker, N. J., Smits, J. J. T., ... & Van Roosmalen, J. A. M. Influence of a TiCl4 post-treatment on nanocrystalline TiO2 films in dye-sensitized solar cells. The Journal of Physical Chemistry B, 2006. 110(39), 19191-19197.
[27] Cojocaru, L., Uchida, S., Sanehira, Y., Nakazaki, J., Kubo, T., & Segawa, H. Surface treatment of the compact TiO2 layer for efficient planar heterojunction perovskite solar cells. Chemistry Letters,2015. 44(5), 674-676.
[28] Murakami, T. N., Miyadera, T., Funaki, T., Cojocaru, L., Kazaoui, S., Chikamatsu, M., & Segawa, H. Adjustment of conduction band edge of compact TiO2 layer in perovskite solar cells through TiCl4 treatment. ACS applied materials & interfaces, 2017. 9(42), 36708-36714.
[29] Tang, Q., Zhang, H., Meng, Y., He, B., & Yu, L. Dissolution engineering of platinum alloy counter electrodes in dye-sensitized solar cells. Angewandte Chemie International Edition, 2015. 54(39), 11448-11452.
[30] Sun, W., Choy, K. L., & Wang, M. The role of thickness control and interface modification in assembling efficient planar perovskite solar cells. Molecules, 2019. 24(19), 3466.
[31] B.C. O' Regan, J.R. Durrant, P.M. Sommeling, N.J. Bakker, Influence of the TiCl4 treatment on nanocrystalline TiO2 films in dye-sensitized solar cells. Charge density, band edge shifts, and quantification of recombination losses at short circuit. J. Phys. Chem. 2007. 111(37), 14001–14010.
[32] Liu, M., Endo, M., Shimazaki, A., Wakamiya, A., & Tachibana, Y. Excitation wavelength dependent interfacial charge transfer dynamics in a CH3NH3PbI3 perovskite film. Journal of Photopolymer Science and Technology,2018. 31(5), 633-642.
[33] Makuta, S., Liu, M., Endo, M., Nishimura, H., Wakamiya, A., & Tachibana, Y. Photo-excitation intensity dependent electron and hole injections from lead iodide perovskite to nanocrystalline TiO 2 and spiro-OMeTAD. Chemical Communications, 2016. 52(4), 673-676.
[34] Wang, E., Chen, P., Yin, X., Gao, B., & Que, W. Boosting efficiency of planar heterojunction perovskite solar cells by a low temperature TiCl4 treatment. Journal of Advanced Dielectrics, 2018. 8(02), 18500098.
[35] Liu, Z., Chen, Q., Hong, Z., Zhou, H., Xu, X., De Marco, N., ... & Yang, Y. Low-temperature TiO x compact layer for planar heterojunction perovskite solar cells. ACS Applied Materials & Interfaces, 2016. 8(17), 11076-11083.
[36] Vesce, L., Riccitelli, R., Soscia, G., Brown, T. M., Di Carlo, A., & Reale, A. Optimization of nanostructured titania photoanodes for dye-sensitized solar cells: Study and experimentation of TiCl4 treatment. Journal of Non-crystalline solids, 2010. 356(37-40), 1958-1961.

[37] Miranda-Gamboa, R. A., Baron-Jaimes, A., Millán-Franco, M. A., Pérez, O., Rincon, M. E., & Jaramillo-Quintero, O. A. Understanding the effect of TiCl4 treatment at TiO2/Sb2S3 interface on the enhanced performance of Sb2S3 solar cells, 2024. Materials Research Express, 11(2), 025003.
[38] Karaoğlan, G. K., Hışır, A., Maden, Y. E., Karakuş, M. Ö., & Koca, A. Synthesis, characterization, electrochemical, spectroelectrochemical and dye-sensitized solar cell properties of phthalocyanines containing carboxylic acid anchoring groups as photosensitizer. Dyes and Pigments, 2022. 204, 110390.
[39] Mehmood, U., Hussein, I. A., Harrabi, K., Tabet, N., & Berdiyorov, G. R. Enhanced photovoltaic performance with co-sensitization of a ruthenium (II) sensitizer and an organic dye in dye-sensitized solar cells. RSC Adv. 2016. 6, 7897–7901.
[40] Mahajan, U., Prajapat, K., Sahu, K., Ghosh, P., Shirage, P. M., & Dhonde, M. Unveiling the impact of TiCl4 surface passivation on dye-sensitized solar cells: enhancing charge transfer kinetics and power conversion efficiency. Journal of Materials Science: Materials in Electronics, 2023. 34(31), 2108.
[41] Ilgün, C., Sevim, A. M., Cakar, S., Özacar, M., & Gül, A. Novel Co and Zn-Phthalocyanine dyes with octa-carboxylic acid substituents for DSSCs. Solar Energy, 2021. 218, 169-179.
[42] Sebuso, D. P., Kuvarega, A. T., Lefatshe, K., King'ondu, C. K., Numan, N., Maaza, M., & Muiva, C. M. Corn husk multilayered graphene/ZnO nanocomposite materials with enhanced photocatalytic activity for organic dyes and doxycycline degradation. Materials Research Bulletin, 2022. 151, 111800.
[43] Bardizza, G., Pavanello, D., Galleano, R., Sample, T., & Müllejans, H. Calibration procedure for solar cells exhibiting slow response and application to a dye-sensitized photovoltaic device. Solar Energy Materials and Solar Cells,2017. 160, 418-424.
[44] Bilen, K. E. M. A. L., & Yildiz, Y. U. S. U. F. Synergistic effect of Ga (NO3) 3 & TiCl4 post-treatment on photovoltaic performance of dye-sensitized solar cells. Applied Physics A, 2023. 129(4), 310.
[45] Srivastava, A., Satrughna, J. A. K., Tiwari, M. K., Kanwade, A., Yadav, S. C., Bala, K., & Shirage, P. M. Effect of Ti 1− x Fe x O 2 photoanodes on the performance of dye-sensitized solar cells utilizing natural betalain pigments extracted from Beta vulgaris (BV). Energy Advances, 2023. 2(1), 148-160.
[46] S.W. Lee, K.S. Ahn, K. Zhu, N.R. Neale, A.J. Frank, Effects of TiCl 4 treatment of nanoporous TiO 2 films on morphology, light harvesting, and charge-carrier dynamics in dye-sensitized solar cells. J. Phys. Chem. C 2012. 116, 21285–21290.
[47] P.R. Schol, W.S. Zhang, T. Scharl, A. Kunzmann, W. Peukert, R.R. Schröder, D.M. Guldi, Intrinsic and extrinsic incorporation of indium and single-walled carbon nanotubes for improved ZnO-based DSSCs. Adv. Energy Mater. 2022. 12(13), 2103662.
[48] Elboughdiri, N., Lakikza, I., Boublia, A., Aouni, S. I., Hammoudi, N. E. H., Georgin, J., ... & Benguerba, Y. Application of statistical physical, DFT computation and molecular dynamics simulation for enhanced removal of crystal violet and basic fuchsin dyes utilizing biosorbent derived from residual watermelon seeds (citrullus lanatus). Process Safety and Environmental Protection 2024. 186, 995-1010.
[49] Q.M. Fu, D.C. He, Z.C. Yao, J.L. Peng, H.Y. Zhao, H. Tao, Z. Chen, Y.F. Tu, Y. Tian, D. Zhou, G. Zheng, Z.B. Ma, Self-powered ultraviolet photodetector based on ZnO nanorod arrays decorated with sea anemone-like CuO nanostructures, Mater. Lett. 2018. 222, 74–77.
[50] S. Sharma, R. Khosla, D. Deva, H. Shrimali, S.K. Sharma, Fluorine-Chlorine codoped TiO2/CSA doped Polyaniline based high performance Inorganic/Organic hybrid heterostructure for UV photodetection applications, Sensor Actuator Phys. 2017. 261, 94–102.